

Accepted Manuscript

Synthetic stratagem and structures of two heteroleptic cobalt(III) complexes acting as biomimetic catalysts: Role of co-ligands in catalytic activities

Kousik Ghosh, Shouvik Chattopadhyay

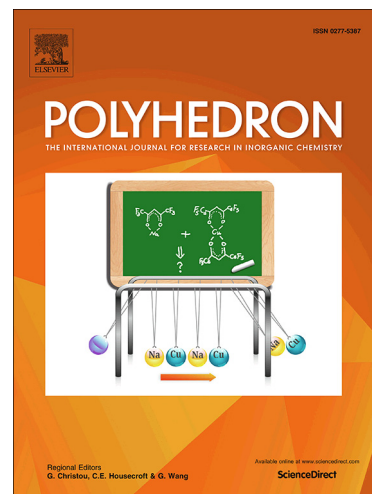
PII: S0277-5387(19)30400-0
DOI: <https://doi.org/10.1016/j.poly.2019.05.062>
Reference: POLY 13987

To appear in: *Polyhedron*

Received Date: 4 May 2019
Revised Date: 28 May 2019
Accepted Date: 30 May 2019

Please cite this article as: K. Ghosh, S. Chattopadhyay, Synthetic stratagem and structures of two heteroleptic cobalt(III) complexes acting as biomimetic catalysts: Role of co-ligands in catalytic activities, *Polyhedron* (2019), doi: <https://doi.org/10.1016/j.poly.2019.05.062>

This is a PDF file of an unedited manuscript that has been accepted for publication. As a service to our customers we are providing this early version of the manuscript. The manuscript will undergo copyediting, typesetting, and review of the resulting proof before it is published in its final form. Please note that during the production process errors may be discovered which could affect the content, and all legal disclaimers that apply to the journal pertain.



Synthetic stratagem and structures of two heteroleptic cobalt(III) complexes acting as biomimetic catalysts: Role of co-ligands in catalytic activities

Kousik Ghosh, Shouvik Chattopadhyay*

Department of Chemistry, Inorganic Section, Jadavpur University, Kolkata 700 032, India

e-mail: shouvik.chem@gmail.com Tel. +91-33- 2414-2941

Abstract

Two heteroleptic cobalt(III) complexes, $[CoL^1(acac)(N_3)]$ (**1**) and $[CoL^1(acac)(NCS)]$ (**2**) {where $HL^1=1-((2-(dimethylamino)ethylimino)methyl)naphthalen-2-ol$, $Hacac = acetylacetonate$,} have been synthesized and structurally characterized by several analytical techniques including single crystal X-ray diffraction analysis. Extended supra-molecular assemblies were generated in them through weak noncovalent interactions. Synthesized complexes have also been found to mimic the role of quite a lot of metalloenzymes like catechol oxidase, phenoxazinone synthase and phosphatase efficiently by catalytic areal oxidation of respective substrates. Detailed kinetic studies of catalytic reactions are performed spectrophotometrically, which confirm that catalytic reactions follow Michaelis-Menten enzymatic reaction kinetics. Role of co-ligands in catalytic activity has also been assessed.

Keywords: Cobalt(III); Schiff base; Crystal structure; Catechol oxidase, phenoxazinone synthase and phosphatase mimicking activity.

1. Introduction

The efficiency and selectivity of various metalloenzymes in processing molecular dioxygen have lead synthetic inorganic chemists to prepare metal complexes and investigate their ability to mimic these enzymes [1-3]. A lot of information regarding the role of metal ions in oxidative and hydrolytic metalloenzymes has been gained through several relative studies on metalloenzymes and synthetic model metal complexes [4-6]. A number of investigations with model complexes have been performed to mimic the structural and functional properties of these metalloenzymes, which confirms that the presence of at least one labile site in the metal complex is essential for binding of the substrate to initiate the catalytic process [7-9]. In one of our previous work, it was shown that mononuclear cobalt(III) complexes of the type $[\text{Co}(\text{ABC})(\text{DE})\text{X}]$ {ABC is a tridentate ligand, DE is a bidentate ligand and X is a pseudo-halide} are showing good catalytic activity due to the presence of easily replaceable pseudo-halide, thereby producing catalytically active intermediate species, $[\text{Co}(\text{ABC})(\text{DE})(\text{substrate})]$ [10]. It was also reported that octahedral bis-ligand cobalt(III) complexes of tridentate N_2O donor Schiff bases were not showing any catalytic activity, as expected [9, 11].

It is to be mentioned here that although mimicking activities of various cobalt(III) complexes have been checked in our previous works [9-11], the change in mimicking activity on changing only the monodentate co-ligand has not been checked. Keeping this fact in mind, we have synthesized two similar complexes differing only in the nature of monodentate pseudo-halides, e.g. azide and thiocyanate. Catalytic activities have been checked and correlated with the ability of monodentate co-ligands to dissociate, thereby initiating catalysis.

In the present work, acetylacetonone (*Hacac*) has been used as a blocking bidentate ligand to form octahedral cobalt(III) complexes of the type, $[\text{CoL}^1(\text{acac})\text{X}]$ with a tridentate N_2O donor Schiff base (*1-((2-(dimethylamino)ethylimino)methyl)naphthalen-2-ol*) and each is having one

easily replaceable pseudo-halide ($X =$ azide for **1** and thiocyanate for **2**). Catechol oxidase, phenoxazinone synthase and phosphatase like activities of synthesized complexes have been inspected using 3,5-di-tert-butylcatechol (3,5-DTBC) *o*-aminophenol (OAPH) and 4-nitrophenylphosphate (4-NPP), as model substrates, respectively, to evaluate their catalytic efficiency and role of the monodentate co-ligands in these catalytic mimicking activities. The higher activity of complex **2** towards these bio-relevant catalyses may be correlated with the ease of releasing co-ligand, thiocyanate (compared to azide) forming stable catalyst-substrate adduct.

2. Material and methods

2.1. Starting materials and solvents

Starting materials and solvents used in this work were purchased from Sigma-Aldrich, India (now Merck, India) and were of reagent grade. They were used as received, without any further purification. The entire syntheses and manipulations were carried out under aerobic conditions.

Caution!!! Even though no troubles were experienced in this work, metal complexes containing azide salts and organic ligands are potentially explosive. Only a small amount of material should be prepared, and it should be handled with care.

2.2. Preparation of $[CoL^1(acac)(N_3)]$ (**1**) [Where, $HL^1 = 1-((2-(dimethylamino)ethylimino)methyl)naphthalen-2-ol]$

A methanol solution (20 ml) of *N,N*-dimethyl-1,2-diaminoethane (0.11 mL, ~1 mmol) and 2-hydroxy-1-naphthaldehyde (172 mg, ~1 mmol) was refluxed for ca. 1 h to prepare tridentate Schiff base ligand, HL^1 . A methanol solution (10 ml) of cobalt(II) acetate tetrahydrate

(250 mg, ~1 mmol) was added into the methanol solution of the Schiff base ligand, HL^1 , under stirring condition to get a dark brown solution. A methanol solution of *acetylacetone* (0.10 mL, ~1 mmol) was added to the resulting dark brown coloured solution, followed by the addition of a methanol–water (10:1) solution of *sodium azide* (65 mg, ~1 mmol) with constant stirring. After leaving the resulting solution in aerial condition to evaporate about half of the solvent, diffraction quality dark brown coloured blocked shaped single crystals of the complex were formed. The crystals were isolated, washed with mother liquor and dried in a vacuum desiccator using anhydrous *calcium chloride*.

Yield: 330 mg (74.6%); based on cobalt(III). Anal. Calc. for $C_{20}H_{25}CoN_5O_3$ (FW = 442.38): C, 54.30; H, 5.70; N, 15.83%. Found: C, 54.2; H, 5.6; N, 15.9%. FT-IR (KBr, cm^{-1}): 3028-2933 (ν_{C-H}), 2016 (ν_{N_3}), 1617 ($\nu_{C=N}$), 1520 ($\nu_{C=O}$), 1440 ($\nu_{C=C}$), 1278 (ν_{C-O}). UV-Vis, λ_{max} (nm), [ϵ_{max} ($dm^3 mol^{-1} cm^{-1}$)] (CH_3CN), 490 (9.22×10^2), 415 (5.31×10^3), 316 (2.73×10^4), 270 (7.24×10^4).

2.3. Preparation of $[CoL^1(acac)(NCS)]$ (2)

Complex **2** was prepared in a similar method as that followed for the preparation of complex **1**, except that *sodium thiocyanate* (81 mg, ~1 mmol) was used instead of *sodium azide*. X-ray quality dark brown single crystals started to grow from methanol solution after several days.

Yield: 340 mg (74.2%); based on cobalt(III). Anal. Calc. for $C_{21}H_{25}CoN_3O_3S$ (FW = 458.43): C, 55.02; H, 5.50; N, 9.17%. Found: C, 54.8; H, 5.3; N, 9.3%. FT-IR (KBr, cm^{-1}): 2995-2874 (ν_{C-H}), 2124 (ν_{N_3}), 1627 ($\nu_{C=N}$), 1514 ($\nu_{C=O}$), 1436 ($\nu_{C=C}$), 1254 (ν_{C-O}). UV-Vis, λ_{max} (nm), [ϵ_{max} ($dm^3 mol^{-1} cm^{-1}$)] 497 (2.29×10^2), 415 (1.21×10^4), 396 (1.19×10^4), 275 (6.89×10^4).

2.4. Details of instrumentation

Single crystal x-ray diffraction was performed using a ‘Bruker SMART APEX II’ diffractometer equipped with graphite-monochromated Mo K α radiation ($\lambda = 0.71073 \text{ \AA}$). More instrumentation details have been given in “Supplementary Information” part.

2.5. Hirshfeld surface analysis

Crystal Explorer [12] was used to calculate Hirshfeld surfaces [13,14] and associated 2D fingerprint plots [15-17] of both complexes. Further details could be found in supplementary information part.

2.6. Catalytic activity and kinetic study

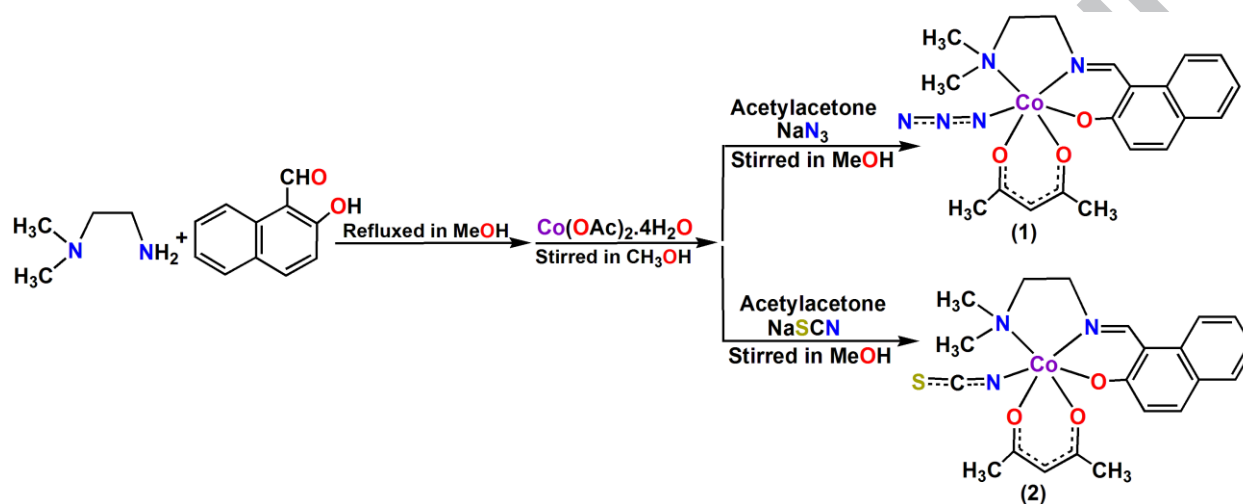
Catechol oxidase, phenoxazinone synthase and phosphatase mimicking activity of both complexes are monitored spectrophotometrically. The additional experimental details of catalytic activity and kinetic study are given in supplementary information part.

3. Results and discussion

3.1 Synthesis of the complexes

The tridentate Schiff base ligand, HL^1 , was prepared by facile condensation of *N,N*-dimethyl-1,2-diaminoethane with 2-hydroxy-1-naphthaldehyde in methanol following the literature method [18-20]. The ligand was not isolated and the yellow coloured methanol solution of the ligand was then reacted with a methanol solution of cobalt(II) acetate tetrahydrate. Addition of acetylacetonone into the resulting solution followed by the addition of aqueous methanol solution of sodium azide produced a mononuclear Schiff base complex, $[CoL^1(acac)(N_3)]$ (**1**). On the contrary, on adding sodium thiocyanate in lieu of sodium azide

produces $[CoL^I(acac)(NCS)]$ (**2**). Cobalt(II) was converted into cobalt(III) by aerial oxidation in presence of (strong field) Schiff base ligand, as observed in many previous cases [9-11]. Use of anaerobic condition prevents the formation of this complex. The formation of the complex is shown in Scheme 1.



Scheme 1: Synthetic route to complexes **1** and **2**.

3.2 Description of solid state structures

3.2.1. Crystal structure of $[CoL^I(acac)(N_3)]$ (**1**) and $[CoL^I(acac)(NCS)]$ (**2**)

Single crystal x-ray structure determination reveals that both complexes consist of discrete mononuclear units having general formula, $[CoL^I(acac)(X)]$, where $X = N_3^-$ (for **1**) and NCS^- (for **2**). Complex **1** crystallizes in monoclinic space group $P2_1/c$, whereas complex **2** crystallizes in monoclinic space group Cc . Perspective views of both complexes with selective atom-numbering scheme are illustrated in Figure 1. Details of the crystallographic data and refinement details of both complexes are given in Table 1. Selected bond lengths and bond angles of both complexes are gathered in Tables 2 and 3 respectively. In each complex,

cobalt(III) centre, *Co(1)*, is coordinated by one imine nitrogen atom, *N(1)*, one amine nitrogen atom, *N(2)*, and one phenoxo oxygen atom, *O(1)*, from one deprotonated Schiff base ligand, (*L*¹)²⁻, and two oxygen atoms, *O(2)* and *O(3)*, of a different ligand, *acac*⁻. Nitrogen atom, *N(3)*, of a terminal azide (in **1**) or thiocyanate (in **2**) occupied the sixth coordination site of *cobalt(III)* centre to complete its distorted octahedral geometry. Bond angles deviate from the ideal values of 90° (for the cis angles) and 180° (for the trans angles), clearly indicate the distortion from perfect octahedral geometry. The saturated five membered chelate ring, [*Co(1)*-*N(1)*-*C(12)*-*C(13)*-*N(2)*], presents in half chair conformation, with puckering parameters [21,22] $Q = 0.414(5) \text{ \AA}$, $\phi = 287.7(5)^\circ$ (for **1**) and $Q = 0.447(3) \text{ \AA}$, $\phi = 90.0(3)^\circ$ (for **2**). The *Co(III)*-*N*_{imine} distances are shorter than the *Co(III)*-*N*_{amine} ones, due to different hybridization of nitrogen atoms. This is a common phenomenon observed in many other *cobalt(III)* Schiff base complexes [9-11]. The terminal azide in **1** and thiocyanate in **2** are quasi-linear with the N-N-N and N-C-S angles being 176.2(4)° and 178.4(3)° respectively, as observed in similar complexes [9-11].

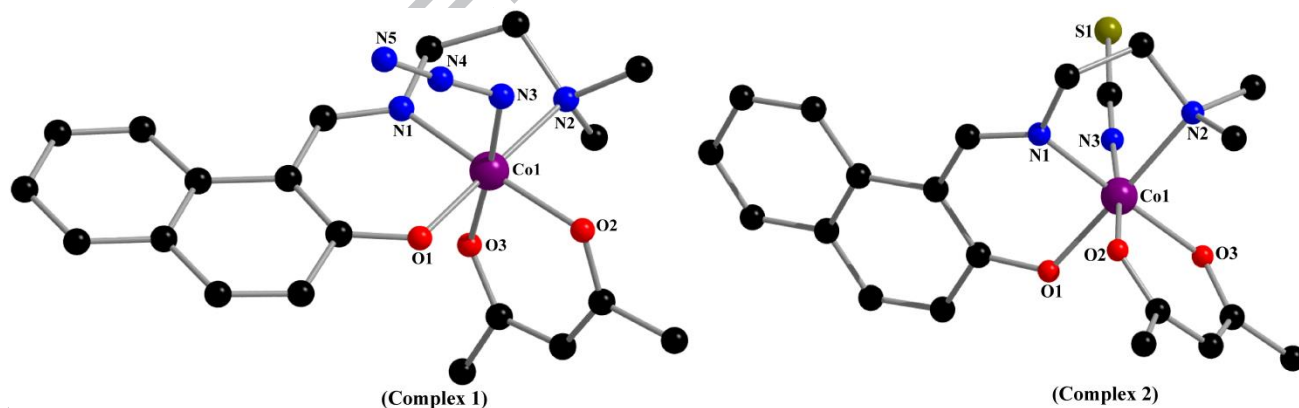


Figure 1: Molecular structure of both complexes with selective atom numbering scheme.

Hydrogen atoms are omitted for clarity.

3.2.2. Significant supramolecular interactions

Significant supramolecular interactions lead to the formation of extended supramolecular architectures in solid state of both complexes. In complex **1**, nitrogen atom, N(5) of terminal azide, is involved in intra-molecular $N\cdots\pi$ interaction with six membered chelate ring, Cg2 [Co(1)-N(1)-C(11)-C(5)-C(6)-O(1)] (Figure 2).

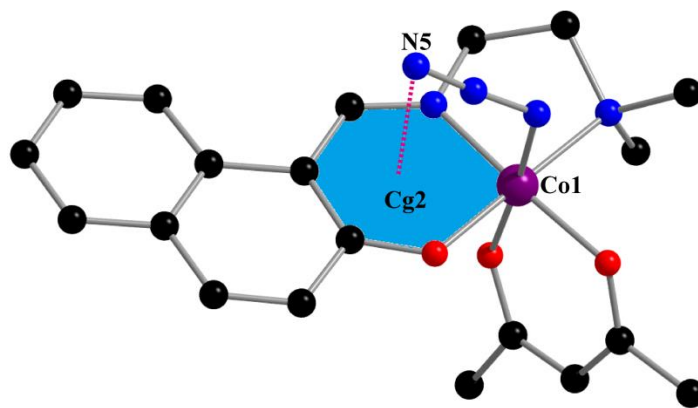


Figure 2: Intra-molecular $N\cdots\pi$ interaction present in complex **1**. Hydrogen atoms are omitted for clarity.

Similarly in complex **2**, hydrogen atom, H(14B), attached with methyl carbon atom, C(14), is involved in intra-molecular $C-H\cdots\pi$ interaction with six membered chelate ring, Cg3 [Co(1)-O(2)-C(17)-C(18)-C(19)-O(3)]. On the other hand, hydrogen atom, H(11), attached to carbon atom, C(11), is involved in inter-molecular $C-H\cdots\pi$ interaction with the symmetry related $(x, 1/2-y, -1/2+z)$ chelate ring, Cg3 [Co(1)-O(2)-C(17)-C(18)-C(19)-O(3)] to form a 1D array. Both the intra-molecular and inter-molecular $C-H\cdots\pi$ interactions are depicted in Figure 3. Geometric features of all of these noncovalent interactions are given in Table 4.

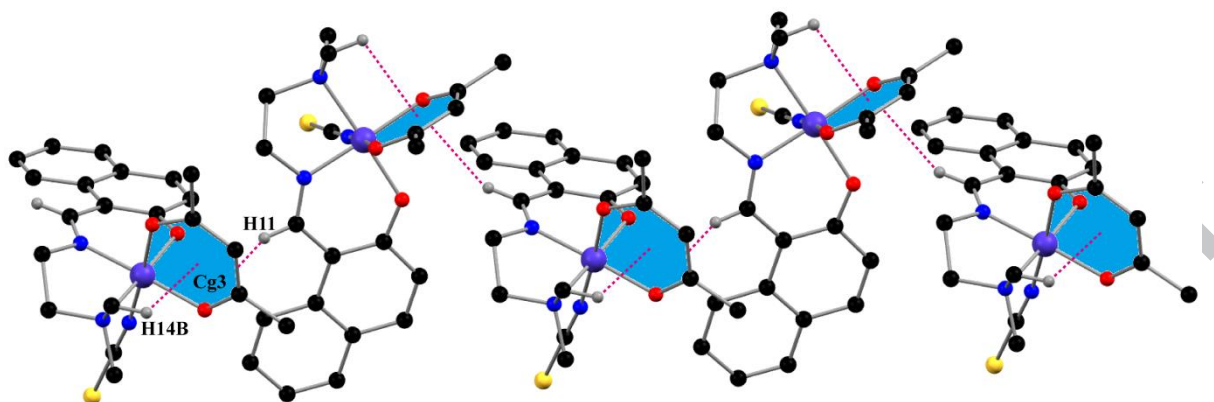


Figure 3: 1D array generated through C-H... π in solid state of complex **2**. Only relevant hydrogen atoms are shown for clarity.

3.3. Hirshfeld surface analysis

Solid state crystal structure of any complex can be determined by an amalgamation of a number of important intermolecular and intramolecular interactions, and hence all these interactions should be taken into account. Hirshfeld surface analysis helps us to visualize and investigate these important supramolecular interactions. Visualization and investigation of these major interactions using Hirshfeld surface based technique symbolize a vital progress in enabling supramolecular chemists and crystal engineers to gain insight into crystal packing. Hirshfeld surfaces of both complexes mapped over d_{norm} , shape index and curvedness (Figure 4). The surfaces are shown as transparent so that molecular moieties around which Hirshfeld surfaces are calculated could be easily picturize. The dominant interactions of both complexes are H...H, C...H/H...C and N...H/H...N (for **1**) or O...H/ H...O (for **2**). Red spots on the d_{norm} surface (Figure 4) indicate that these interactions are dominant. Furthermore, 2D fingerprint plots (Figure 5) exemplify various inter-molecular interaction patterns associated with both complexes and their relative contributions are given in percentage scale. In 2D fingerprint plots inter-

molecular interactions become visible as distinct spikes. Complementary regions are visible in the two dimensional fingerprint plots where one molecule act as donor ($d_e > d_i$) and the other as an acceptor ($d_e < d_i$). The fingerprint plots can also be decomposed to highlight preferred atoms pair close contacts. This decomposition enables separation of contributions from different interaction types, which overlap in the full fingerprint [23].

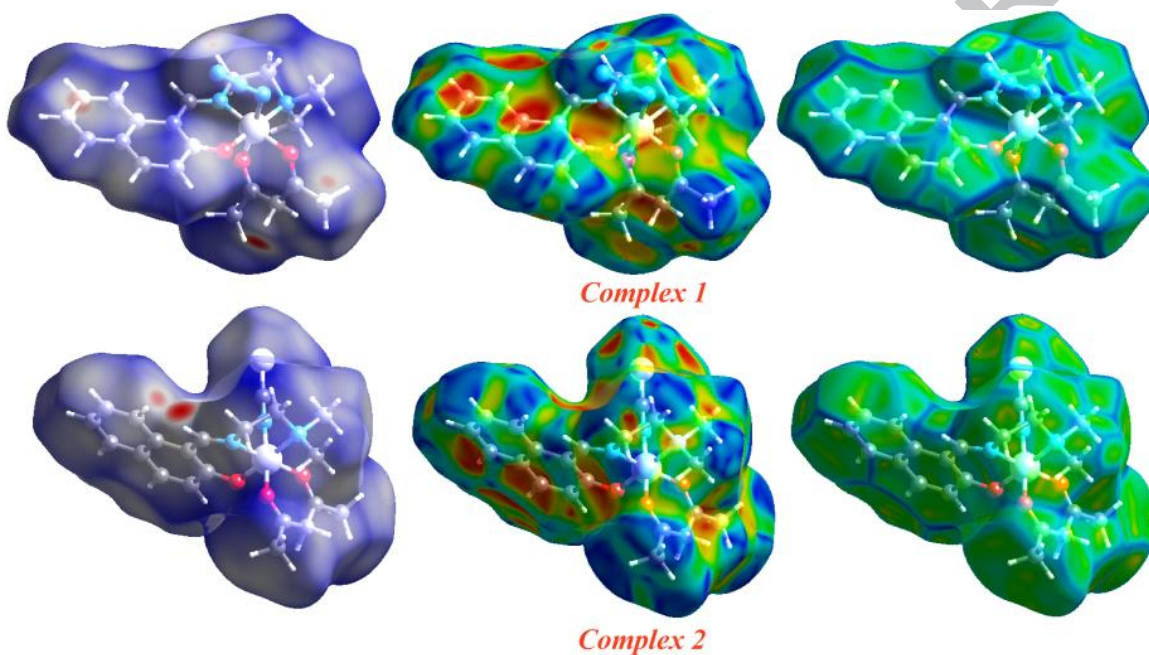


Figure 4: Hirshfeld surfaces mapped over d_{norm} (left-side), shape index (middle) and curvedness (right-side).

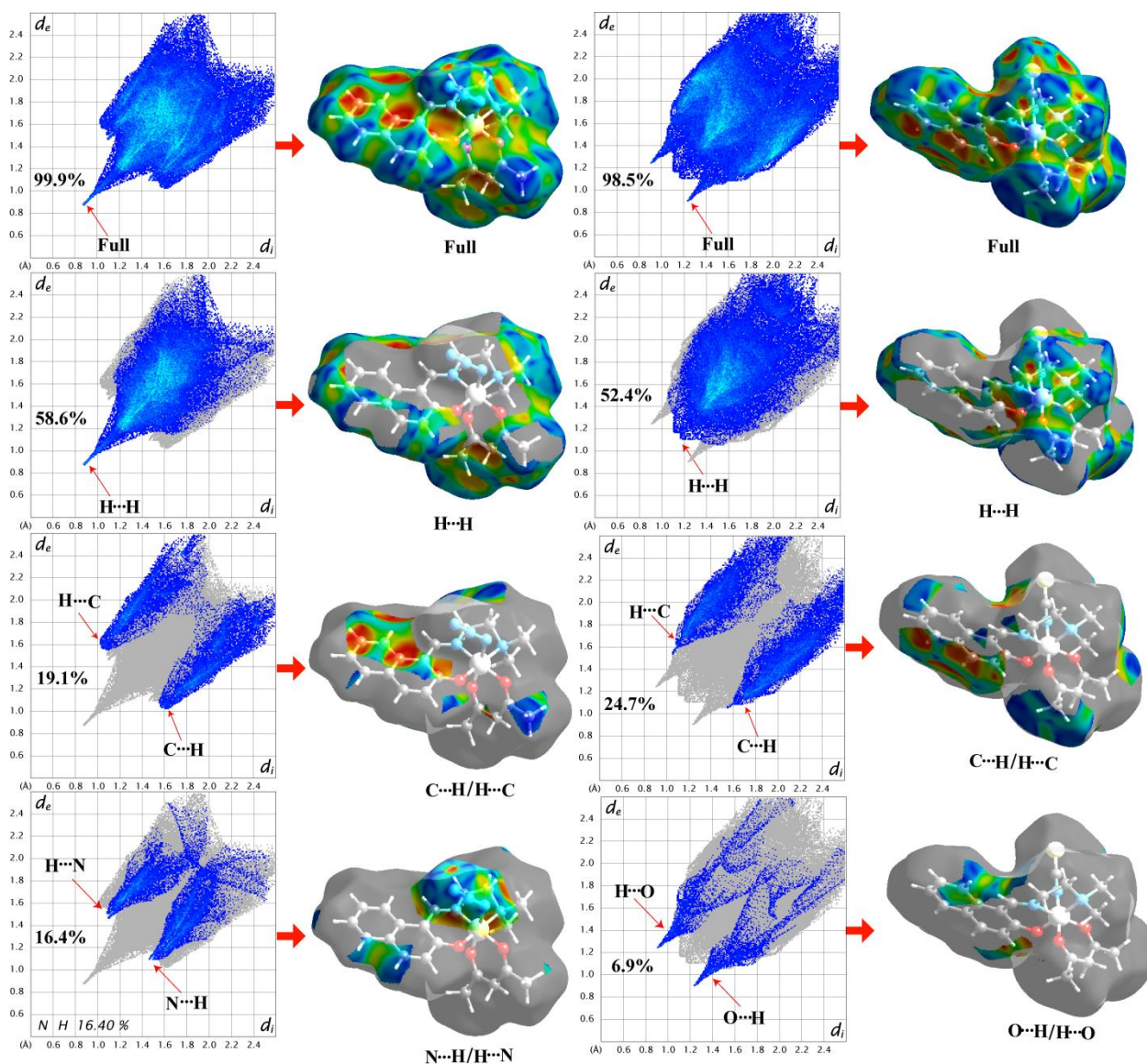


Figure 5: Fingerprint plots of **1** (left-side) and **2** (right-side): full and resolved into H··H, C··H/H··C, N··H/H··N or O··H/H··O contacts showing the percentages of contacts contributed to the total Hirshfeld surface area of both complexes. Surfaces in the right hand columns highlight the relevant surface patches associated with the specific contacts in the total Hirshfeld surface area of both complexes.

3.4. IR and electronic spectroscopy

The IR and electronic spectra of both complexes are in sound agreement with the findings obtained from x-ray crystallography. In IR spectra of both complexes, characteristic absorption bands corresponding to azomethine ($>C=N^-$) groups are observed at 1617 (for **1**) and 1627 cm^{-1} (for **2**) [9-11]. These bands are shifted to somewhat lower frequencies due to the coordination of the azomethine group with the metal centre. Both complexes show strong bands around 1520 cm^{-1} due to the presence of keto group ($C=O$) and moderately strong band around 1270 cm^{-1} due to the presence of C-O (phenoxy) stretching [10]. Sharp absorption bands at 2016 cm^{-1} (in **1**) or 2124 cm^{-1} (in **2**) indicate the presence of terminal azide (for **1**) and N-bonded thiocyanate (for **2**) respectively, which are also evident from crystal structure determination [9]. In addition, the IR spectrum of both complexes also exhibits several weak bands for the aromatic and aliphatic C-H stretching vibration frequencies in the region 3080-2874 cm^{-1} [9-11], and strong bands for the aromatic C=C stretching bonds around 1440 cm^{-1} [24].

Electronic absorption spectra of both complexes in acetonitrile medium shows d-d transition bands around 490 and 415 nm, as expected for a low spin cobalt(III) complex in octahedral geometry [24,25]. Broad absorption bands at 316 nm (for **1**) and 396 nm (for **2**) are also observed which is consistent with LMCT band [24,25]. Additionally, high energy absorption bands around 270 nm may be attributed to intra-ligand transitions i.e. $\pi \rightarrow \pi^*$ and $n \rightarrow \pi^*$ transitions [24,25].

3.5. Catechol oxidase and phenoxazinone synthase mimicking activity

The catechol oxidase mimicking activity of synthesized complexes has been evaluated using 3,5-DTBC as a model substrate due to its easy oxidation to 3,5-di-tert-butylbenzoquinone (3,5-DTBQ), whereas OAPH has been used as model substrate for evaluating phenoxazinone

synthase mimicking activity of both complexes. Mimicking activity studies were performed in acetonitrile medium because complexes, substrates and their products are highly soluble in acetonitrile. Entire mimicking activity studies were carried out in absence of any supplementary base to minimize the possibility of oxidation of substrates by molecular dioxygen. Progresses of the reactions were followed spectrophotometrically. Spectrophotometric scans revealed a gradual increase in intensity of the absorption band at ~400 nm (characteristic for 3,5-DTBQ) or ~433 nm (characteristic for phenoxazinone chromophore) for catechol oxidase or phenoxazinone synthase like activities respectively. The resulting solutions were also monitored spectrophotometrically after 48 h, which show the formation of 3,5-DTBQ or 2-aminophenoxazine-3-one respectively as the sole product. These results undoubtedly indicate that synthesized complexes are active towards both catechol oxidase and phenoxazinone synthase mimicking activities. Blank experiments for both of these mimicking activities were also performed under identical conditions and in each case, no significant growth of the absorption bands around was observed at desired wavelengths.

3.6. Phosphatase mimicking activity

The complexes were also utilized as catalyst for hydrolysis of 4-nitrophenylphosphate (4-NPP) to 4-nitrophenolate at room temperature. The catalytic activity was performed in aqueous DMF (98% DMF, v/v) medium because of very good solubility of both 4-NPP and 4-nitrophenolate. Efficiency of P-O bond cleavage of both complexes were evaluated by monitoring the spectral change in the wavelength scan (300-500 nm) of a mixture solution for 2 h where complex to substrate ratio is maintained roughly 1:100 stoichiometrically. Band maxima at ~425 nm confirm formation of 4-nitrophenolate ion. The resulting solutions were also monitored spectrophotometrically after 48 h which show the formation of 4-nitrophenolate as the

sole product with no further increase of band maxima. These consequences clearly indicate that the complexes are active towards phosphatase mimicking activity. Blank experiments without any catalyst were also carried out under identical conditions and in this case, no significant growth of the absorption bands around 425 nm was observed.

3.7. Kinetic investigations through a number of enzyme kinetic plots

The Michaelis-Menten model is the best-known approach for treating biochemical reactions involving a single substrate. Initial rate of the reaction versus substrate concentration was plotted for all of these mimicking activities. These plots suggest rate saturation kinetics. The initial rate of the reaction was calculated by multiplying the substrate concentration with rate constant. Rate constant of the reaction was obtained from the slope of the product concentration vs. time plot. Linearization of Michaelis-Menten equation produces a double reciprocal Lineweaver-Burk plot, which can be used to analyze kinetic parameters like V_{\max} and K_M directly. Additionally, rearrangement of Michaelis-Menten equation gives Hanes equation. In this case, the ratio of the substrate concentration to the reaction rate is plotted against substrate concentration. Eadie-Hofstee equation is sometimes used in biochemistry for a graphical representation of enzyme kinetics. In this plot reaction rate is plotted as a function of the ratio between reaction rate and substrate concentration. All these plots are used to evaluate various kinetic parameters including k_{cat} and specificity constant (k_{cat}/K_M) for catechol oxidase, phenoxazinone synthase and phosphatase mimicking activity of both complexes. The k_{cat} value is obtained by dividing V_{\max} by the concentration of the catalyst (complex) used [9-11]. Figures 6 and 7 represent the Lineweaver-Burk plot, Hanes plot and Eadie-Hofstee plot of complex 2 for catechol oxidase and phenoxazinone synthase mimicking activity, respectively. Similarly, the Lineweaver-Burk plot, Hanes plot and Eadie-Hofstee plot for phosphatase mimicking activity of

complex **2** are illustrated in Figure 8. All these plots of complex **1** are given Figure S2-S4 (Supplementary information). A number of kinetic parameters for catechol oxidase, phenoxazinone synthase and phosphatase mimicking activity of both complexes are gathered in Tables 5, 6 and 7, respectively.

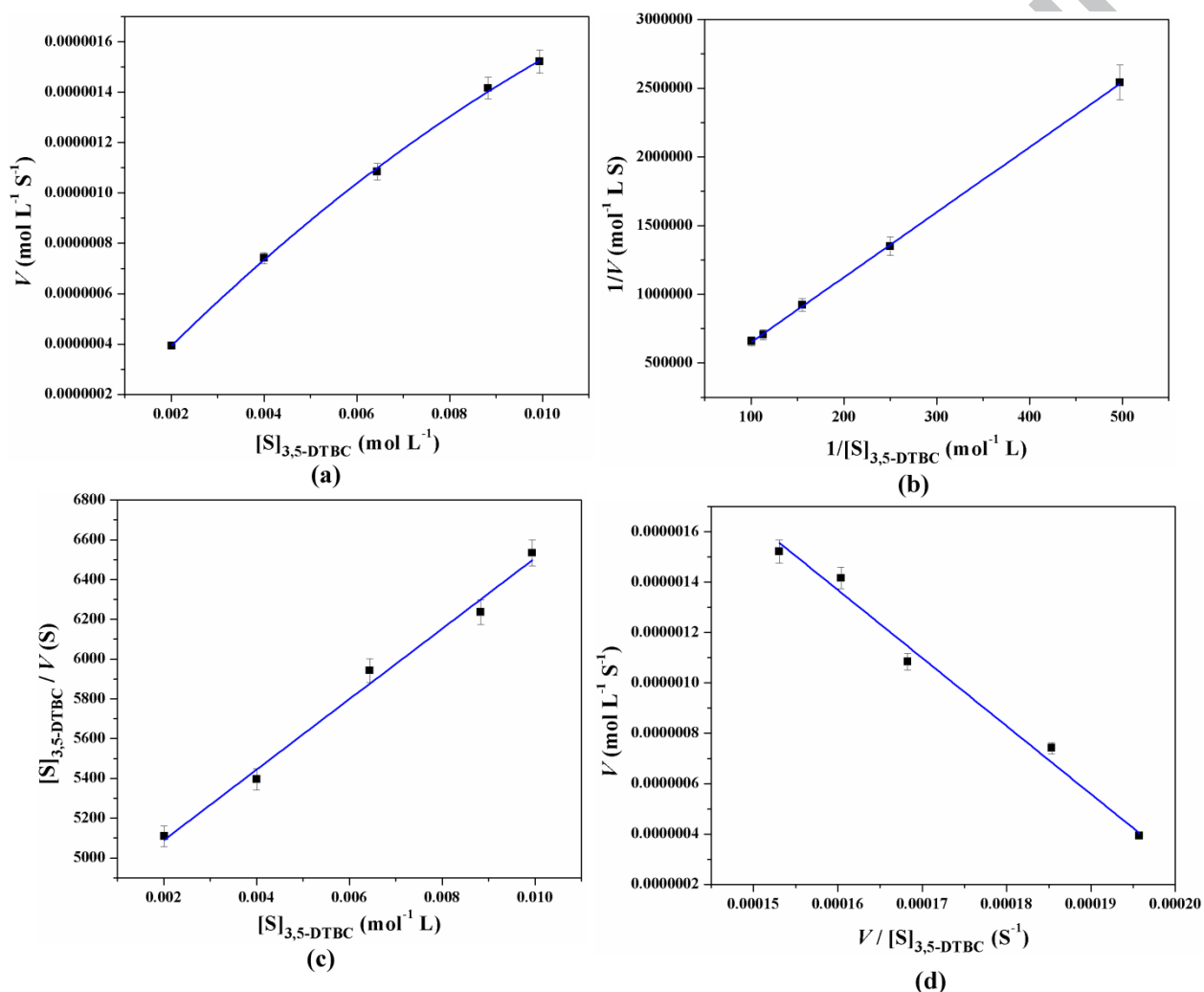


Figure 6: Michaelis-Menten plot (a), Lineweaver-Burk plot (b), Hanes-Woolf plot (c) and Eadie-Hofstee plot (d) of complex **2** for catechol oxidase mimicking activity.

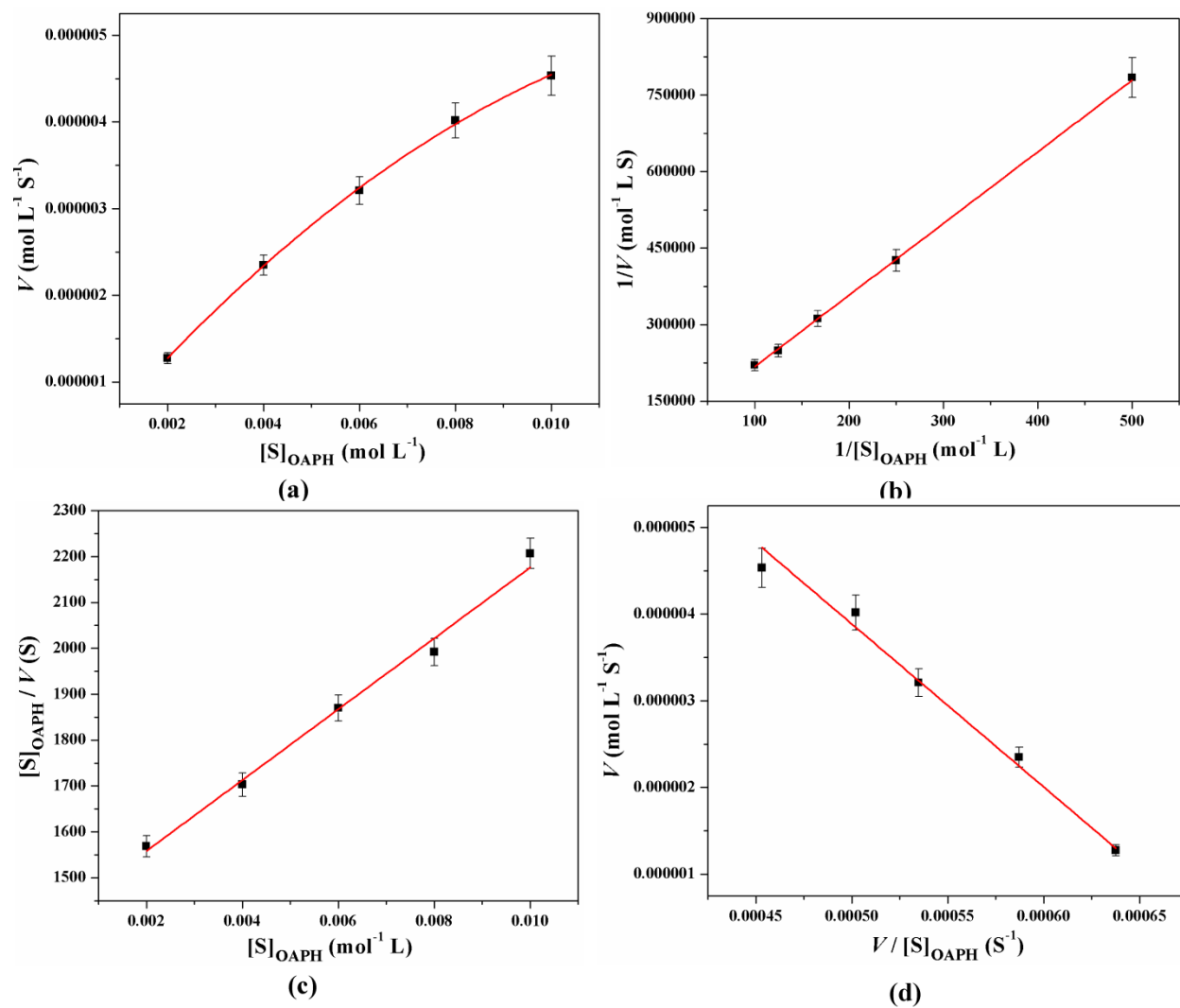


Figure 7: Michaelis-Menten plot (a), Lineweaver-Burk plot (b), Hanes-Woolf plot (c) and Eadie-Hofstee plot (d) of complex **2** for phenoxazinone synthase mimicking activity.

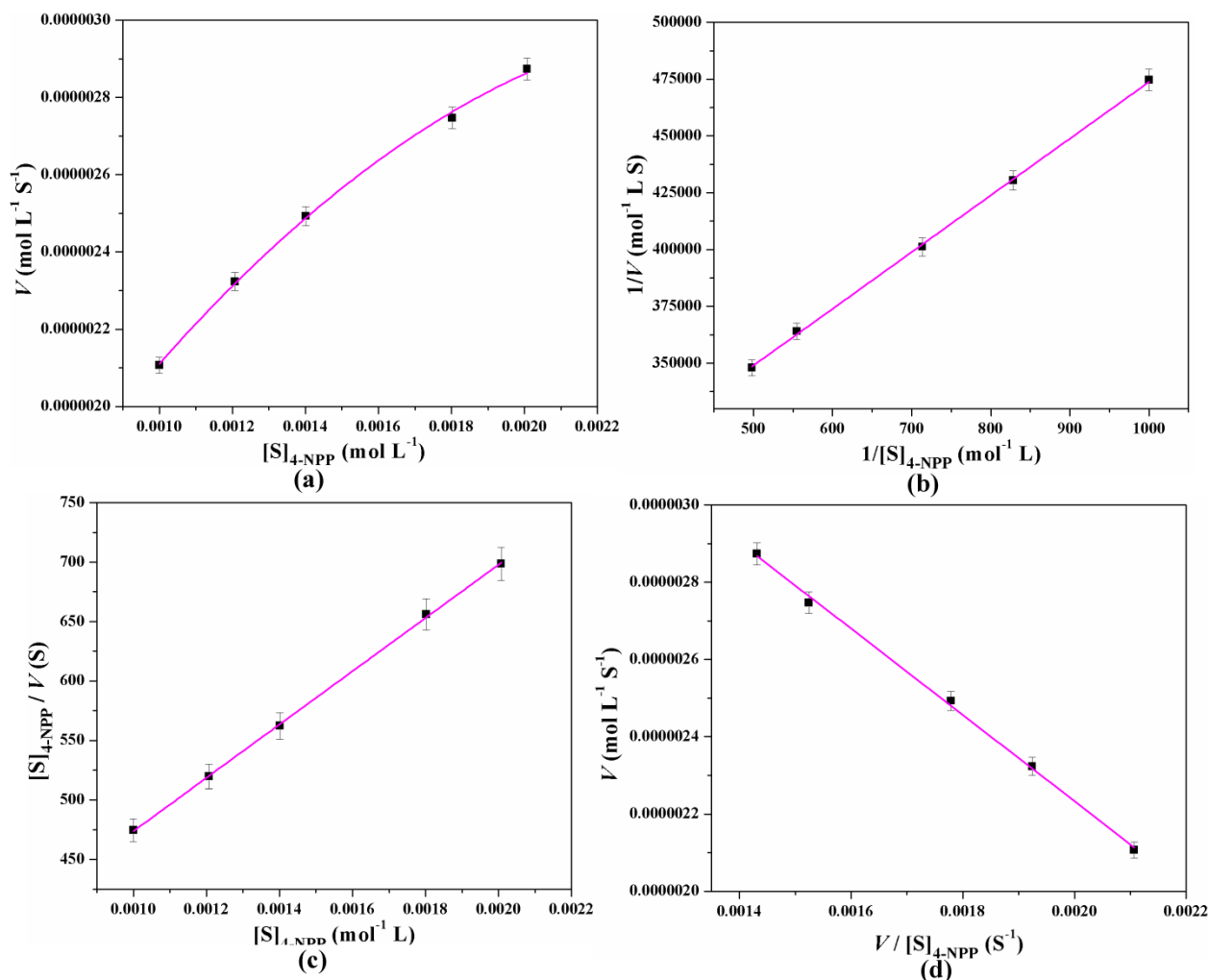
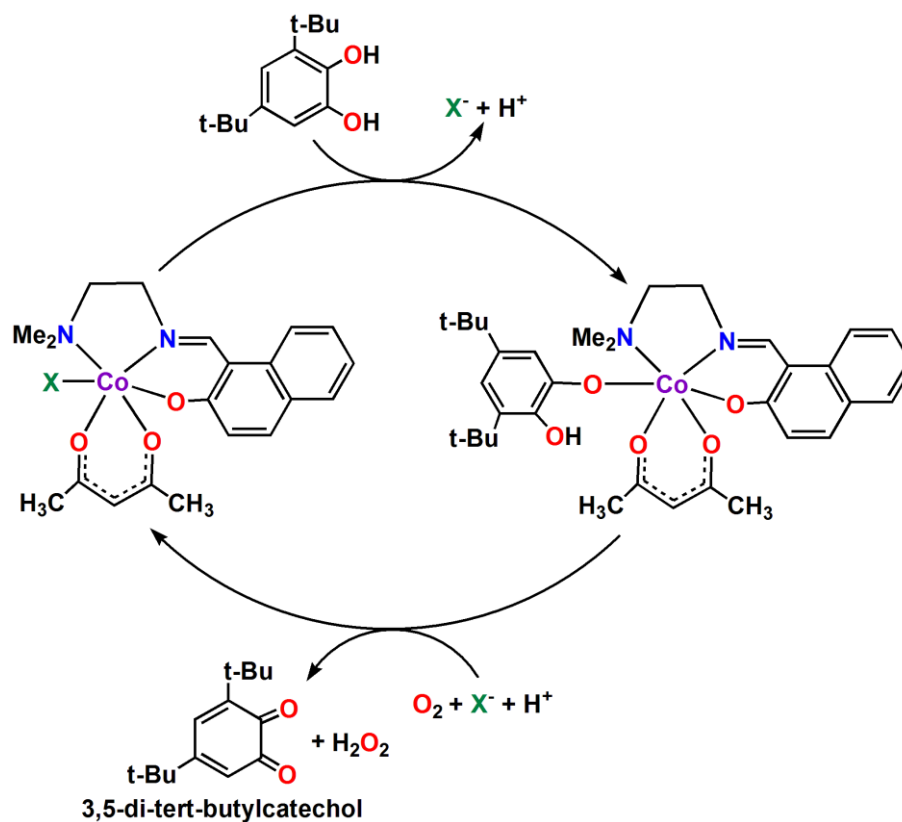


Figure 8: Michaelis-Menten plot (a), Lineweaver-Burk plot (b), Hanes-Woolf plot (c) and Eadie-Hofstee plot (d) of complex 2 for phosphatase mimicking activity.

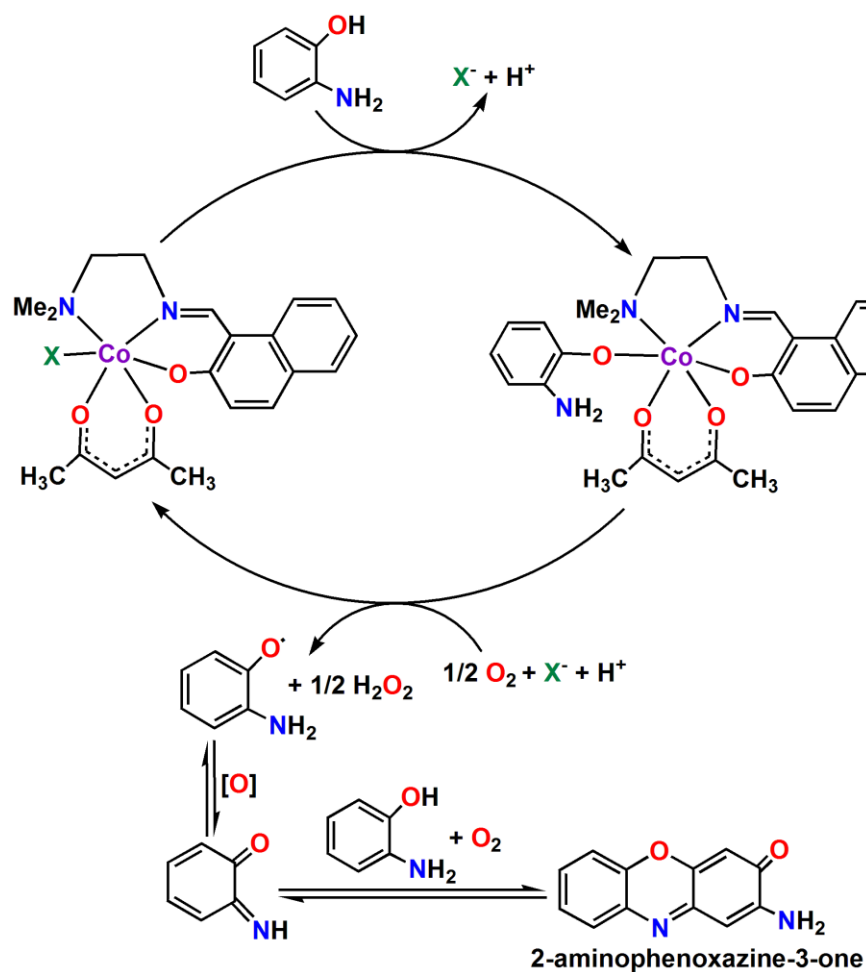
3.8. Mechanistic pathway of catalytic activity

From the experimental results, it is clear that both complexes are able to mimic catechol oxidase, phenoxazinone synthase and phosphatase like enzymes effectively. It is very obvious that quite a few factors may influence the catalytic activity, such as the variable oxidation state of the metal, coordination geometry around the metal centre, metal-metal distance, ligand flexibility, exogenous bridging ligand etc [26,27]. Based on the several previously published

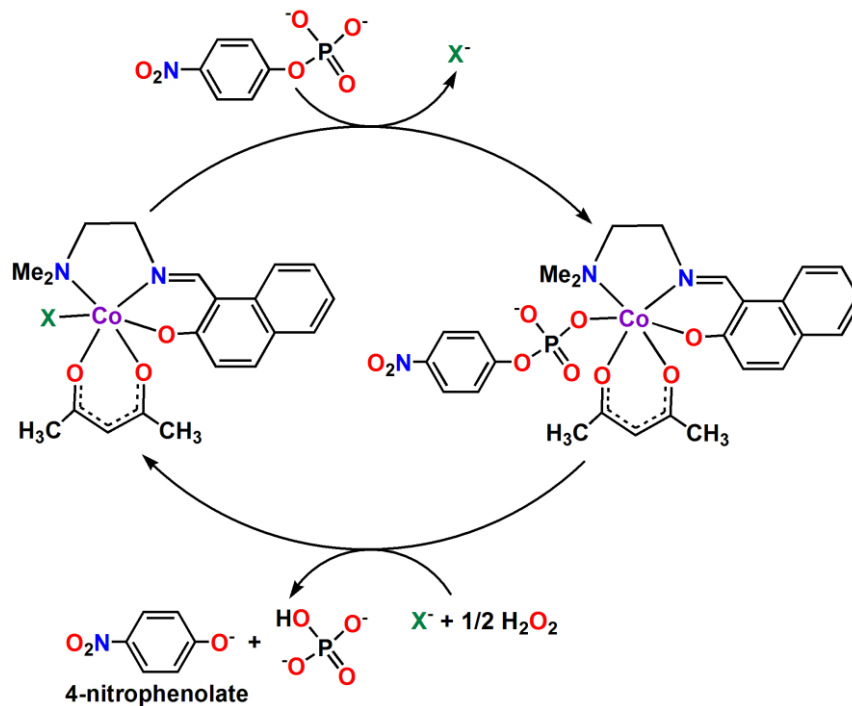
reports [26-30], tentative catalytic conversions for catechol oxidase, phenoxazinone synthase and phosphatase mimicking activities are given in Schemes 2, 3 and 4, respectively.



Scheme 2: Possible mechanistic pathway for catechol oxidase mimicking activity of synthesized complexes.



Scheme 3: Tentative mechanistic pathway for phenoxazinone synthase mimicking activity of synthesized complexes.



Scheme 4: Plausible mechanistic pathway for phosphatase mimicking activity of synthesized complexes.

It can easily be predicted that initially a catalyst-substrate adduct is formed by replacing the monodentate azide or thiocyanate coligand, which subsequently leads to respective products, regenerating catalyst molecules. Catalytic activities depend upon the interaction between substrate and catalyst. Higher the interaction between substrate and catalyst, higher is the k_{cat} values. Interaction between the Catalyst and OAPH molecule is more than that of catalyst and 3,5-DTBC or 4-NPP, as less steric hindrance occur in case of OAPH. That's why the turnover number (k_{cat}) values for phenoxazinone synthase mimicking activity of both complexes are greater than catechol oxidase and phosphatase mimicking activity. It is very clear that, complex **2** acts as more active catalyst than complex **1**. Most probably, this is due to the fact that thiocyanate coligands are much more labile compared to azide. Therefore, substrates can form

catalyst-substrate adduct replacing thiocyanate from complex **2** with greater ease, initiating catalysis. This was found in some of our previous works too [9,10].

To elucidate active species present in catalytic pathways during mimicking activities, the electron spray ionization mass spectrometry of the 1:50 mixtures of complexes and respective substrates has been performed in the positive mode. Complex **2** was taken as a model complex as it exhibits highest k_{cat} value. ESI-MS positive spectra of 1 : 50 mixtures of the complex **2** with 3,5-DTBC, *o*-aminophenol and 4-NPP were recorded separately after 5 min from mixing and the results are depicted in Figures **9**, **10** and **11**, respectively. In presence of 3,5-DTBC, the mass spectrum exhibits a peak at $m/z = 243.0888$, corresponding to quinone sodium aggregate $[(3,5\text{-DTBQ})(\text{Na})]^+$, which confirms the termination of the catalytic cycle. Similarly, the mass spectrum of complex **2** and *o*-aminophenol shows a peak at $m/z = 242.2386$, corresponding to the formation of Na and Li adduct of the deprotonated form of 2-aminophenoxazin-3-one, confirming the phenoxazinone synthase mimicking activity of the complex. On the other hand, mass spectral analysis of complex **2** and 4-NPP confirms the presence of $[(4\text{-nitrophenolate})(\text{Li})(\text{K})]^+$, which is indicated by the appearance of a peak at $m/z = 184.14$. From this mass spectral analysis, phosphatase mimicking activity of the complex has been confirmed. In each case, a peak is observed at $m/z \approx 399$, which may be assigned as $[\text{Co}(\text{L}^1)(\text{acac})]^+$, generated via the loss of monodentate azide/thiocyanate coligand in the initial step of the catalysis. So it is clear that axially coordinated azide/monodentate coligand can easily be replaced. Mass spectral data of complex **1** is exactly similar with the above mention data, indicating similar path of reaction in each catalytic reaction. The mechanistic pathways shown in Schemes **2**, **3** and **4** are therefore justified by the mass spectral analysis.

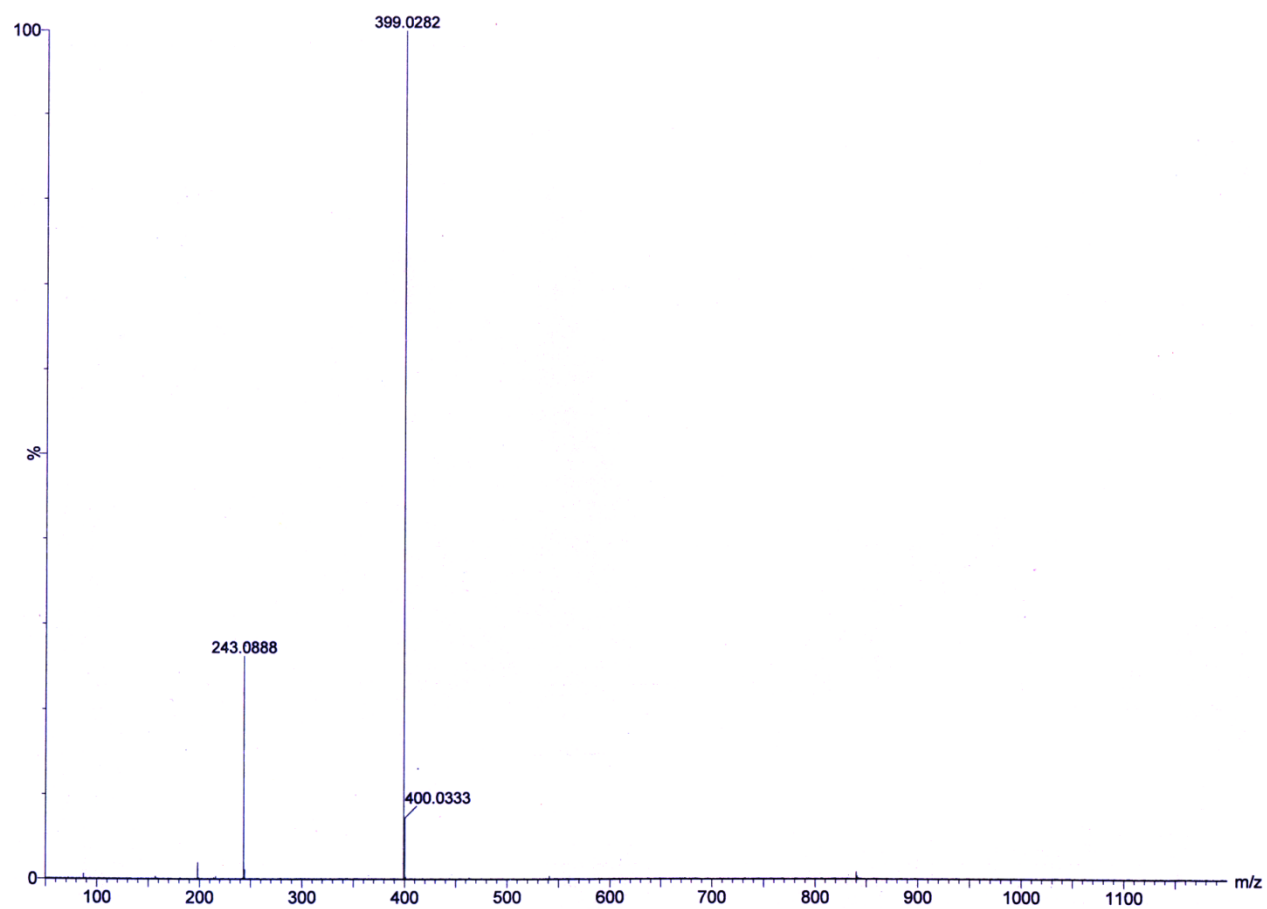


Figure 9: ESI-MS positive spectrum of 1 : 50 mixture of complex **2** and 3,5-DTBC in acetonitrile medium at room temperature.

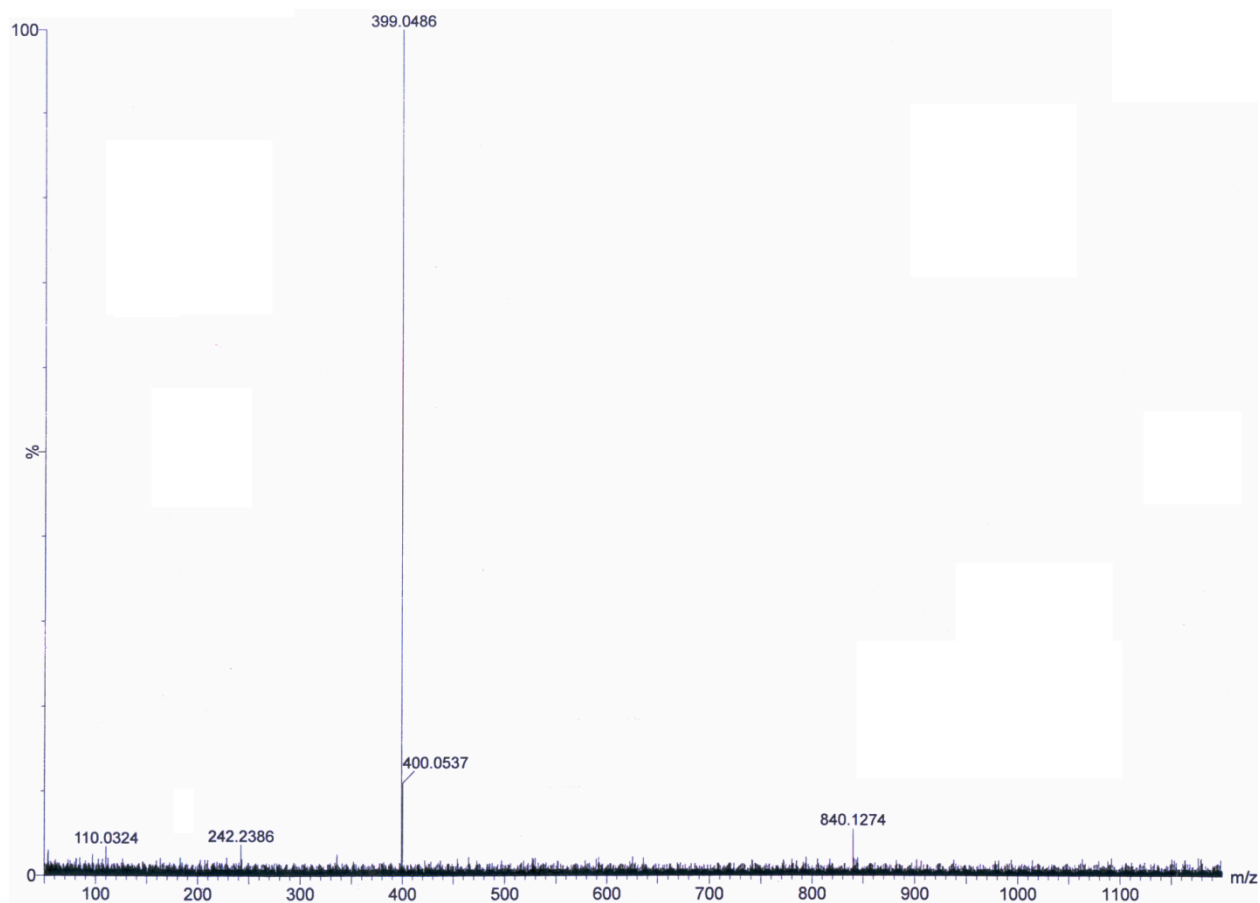


Figure 10: ESI-MS positive spectrum of 1 : 50 mixture of complex **2** and OAPH in acetonitrile medium at room temperature.

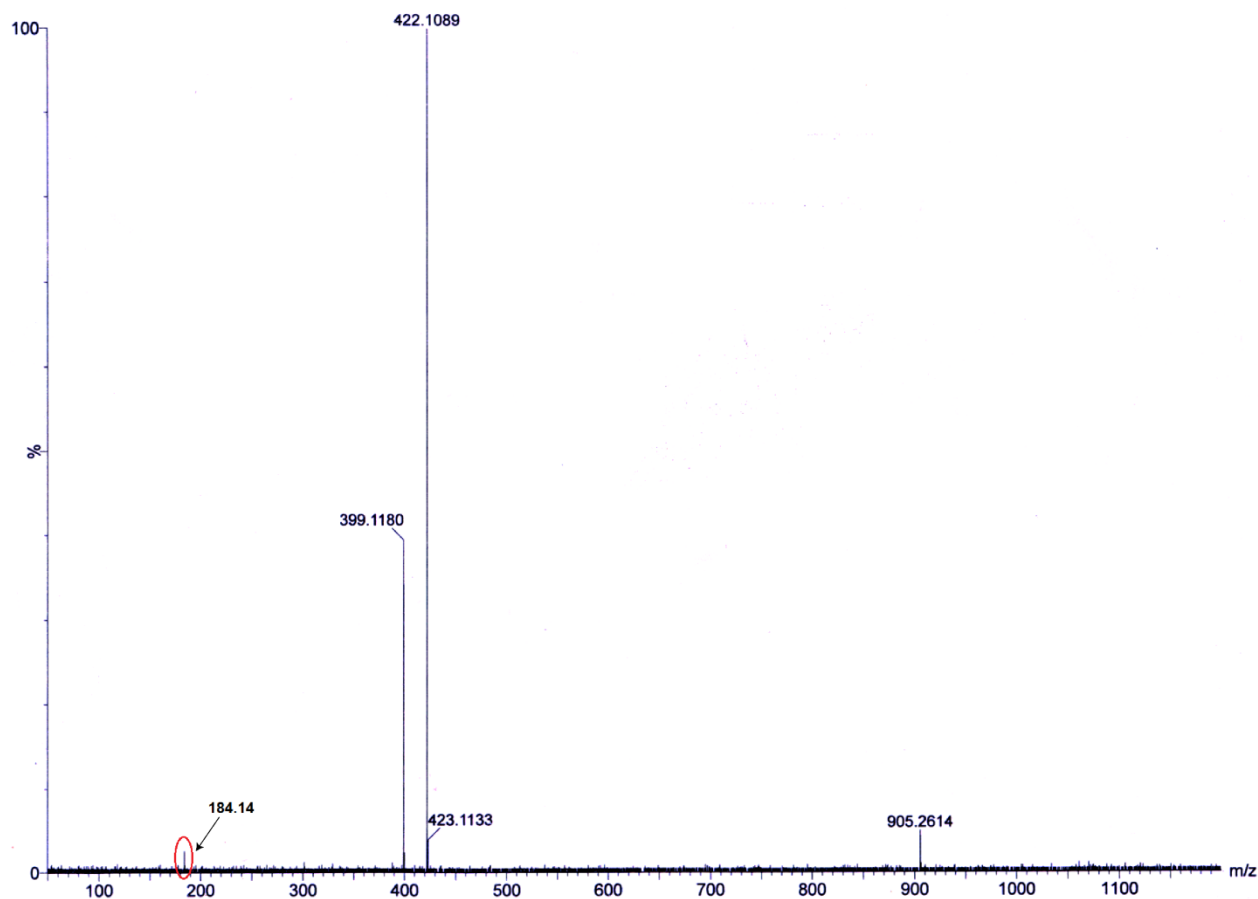


Figure 11: ESI-MS positive spectrum of 1 : 50 mixture of complex **2** and 4-NPP in DMF-water mixture at room temperature.

4. Concluding Remarks

In conclusion, we have discussed the synthetic stratagem and structural characterization of two heteroleptic cobalt(III) complexes. Structures of both complexes have been confirmed by single crystal X-ray diffraction technique. Significant solid state supramolecular interactions in them are also investigated. Synthesized complexes are active towards catalytic conversion of 3,5-DTBC to 3,5-DTBQ (catechol oxidase mimicking activity) and OAPH to 2-aminophenoxazine-3-one (phenoxazinone synthase mimicking activity) in acetonitrile medium. Both complexes have also been found to mimic the role of phosphatase enzyme efficiently by

transforming 4-nitrophenylphosphate to 4-nitrophenolate at room temperature in aqueous DMF (98% DMF, v/v) medium. Mimicking activities have been assessed by following conventional Michaelis-Menten enzymatic kinetics. Kinetic studies of the catalytic cycles have been performed in detail using a variety of enzyme kinetics plots to calculate a number of kinetic parameters, including k_{cat} . The catalytic activity of complex **2** (towards all these bio-relevant catalyses) is higher compared to complex **1**. This may be correlated with the presence of easily replaceable thiocyanate in **2** (compared to azide in **1**) initiating the catalytic cycle by forming stable catalyst-substrate adduct easily.

Acknowledgements

K.G. expresses his gratitude to UGC, India, for awarding a Senior Research Fellowship. Crystallographic data were collected at the DST-FIST, India funded Single Crystal Diffractometer Facility at the Department of Chemistry, Jadavpur University.

Appendix A. Supplementary data

CCDC 1913920-1913921 contain the supplementary crystallographic data of the synthesized complexes. These data can be obtained free of charge via <http://www.ccdc.cam.ac.uk/conts/retrieving.html>, or from the Cambridge Crystallographic Data Centre, 12 Union Road, Cambridge CB2 1EZ, UK; fax: (+44) 1223-336-033; or e-mail: deposit@ccdc.cam.ac.uk.

References:

- [1] F. Natri, M. Chino, O. Maglio, A. Bhagi-Damodaran, Y. Lu, A. Lombardi, *Chem. Soc. Rev.* 45 (2016) 5020-5054.

- [2] M. Fontecave, J. -L. Pierre, *Coord. Chem. Rev.* 170 (1998) 125-140.
- [3] D. J. Xuereb, R. Raja, *Catal. Sci. Technol.* 1 (2011) 517-534.
- [4] M. Zhao, H. -B. Wang, L. -N. Ji, Z. -W. Mao, *Chem. Soc. Rev.* 42 (2013) 8360-8375.
- [5] A. S. Borovik, *Acc. Chem. Res.* 38 (2005) 54-61.
- [6] E. Y. Tshuva, S. J. Lippard, *Chem. Rev.* 104 (2004) 987-1012.
- [7] N. Sarkar, K. Harms, A. Frontera, S. Chattopadhyay, *New J. Chem.* 41 (2017) 8053-8065.
- [8] S. Purkait, P. Chakraborty, A. Frontera, A. Bauzá, E. Zangrando, D. Das, *New J. Chem.* 42 (2018) 12998-13009.
- [9] K. Ghosh, S Roy, A. Ghosh, Abhisek Banerjee, A. Bauzá, A. Frontera, S. Chattopadhyay, *Polyhedron* 112 (2016) 6-17.
- [10] K. Ghosh, K. Harms, S. Chattopadhyay, *ChemistrySelect* 2 (2017) 8207-8220.
- [11] K. Ghosh, K. Harms, S. Chattopadhyay, *Polyhedron* 123 (2017) 162-175.
- [12] S. K. Wolff, D. J. Grimwood, J. J. McKinnon, D Jayatilaka, M. A. Spackman, *Crystal Explorer 2.0*; University of Western Australia: Perth, Australia, (2007).
<http://hirshfeldsurfacenet.blogspot.com/>.
- [13] M. A. Spackman, D. Jayatilaka, *CrystEngComm* 11 (2009) 19-32.
- [14] H. F. Clausen, M. S. Chevallier, M. A. Spackman, B. B. Iversen, *New J. Chem.* 34 (2010) 193-199.

- [15] A. L. Rohl, M. Moret, W. Kaminsky, K. Claborn, J. J. McKinnon, B. Kahr, *Cryst. Growth Des.* 8 (2008) 4517-4525.
- [16] A. Parkin, G. Barr, W. Dong, C. J. Gilmore, D. Jayatilaka, J. J. McKinnon, M. A. Spackman, C. C. Wilson, *CrystEngComm* 9 (2007) 648-652.
- [17] M. A. Spackman, J. J. McKinnon, *CrystEngComm* 4 (2002) 378-392.
- [18] P. Pandey, A. Verma, K. Bretosh, J. -P. Sutter, S. S. Sunkari, *Polyhedron* 164 (2019) 80-89.
- [19] Y. Zhang, M. Avdeev, J. R. Price, I. Karatchevtseva, D. J. Fanna, I. Chironi, K. Lu, *Polyhedron* 165 (2019) 125-131.
- [20] B. -B. Tang, X. -P. Sun, G. -L. Liu, H. Li, *J. Mol. Struct.* 984 (2010) 111-116.
- [21] D. Cremer, J. A. Pople, *J. Am. Chem. Soc.* 97 (1975) 1354-1358.
- [22] A. D. Hill, P. J. Reilly, *J. Chem. Inf. Model.* 47 (2007) 1031-1035.
- [23] M. A. Spackman, P. G. Byrom, *Chem. Phys. Lett.* 267 (1997) 215-220.
- [24] K. Ghosh, K. Harms, A. Bauzá, A. Frontera, S. Chattopadhyay, *Dalton Trans.* 47 (2018) 331-347.
- [25] K. Ghosh, K. Harms, A. Bauzá, A. Frontera, S. Chattopadhyay, *CrystEngComm* 20 (2018) 7281-7292.
- [26] A. Hazari, A. Das, P. Mahapatra, A. Ghosh, *Polyhedron* 134 (2017) 99-106.
- [27] K. Ghosh, K. Harms, A. Franconetti, A. Frontera, S. Chattopadhyay, *J. Organomet. Chem.* 883 (2019) 52-64.
- [28] J. Adhikary, I. Majumdar, P. Kundu, H. Kornweitz, H. Kara, D. Das, *ChemistrySelect* 3 (2018) 1445-1454.

[29] M. Mitra, P. Raghavaiah, R. Ghosh, *New J. Chem.* 39 (2015) 200-205.

[30] K. Ghosh, A. Banerjee, A. Bauzá, A. Frontera, S. Chattopadhyay, *RSC Adv.* 8 (2018) 28216-28237.

ACCEPTED MANUSCRIPT

Table 1: Crystal data and refinement details of complexes **1** and **2**.

	Complex 1	Complex 2
Formula	C ₂₀ H ₂₅ CoN ₅ O ₃	C ₂₁ H ₂₅ CoN ₃ O ₃ S
Formula Weight	442.38	458.43
Temperature (K)	296(2)	296(2)
Crystal System	Monoclinic	Monoclinic
Space group	<i>Cc</i>	<i>P2₁/c</i>
a(Å)	7.7642(3)	9.5965(5)
b(Å)	18.2919(8)	19.6256(10)
c(Å)	14.3215(5)	11.8519(6)
β(°)	98.123(2)	103.215(3)
D(calc) [g/cm ³]	1.459	1.401
μ [mm ⁻¹]	0.884	0.912
F(000)	924	956
Total Reflections	14053	31576
Unique Reflections	3811	3979
Observed data [<i>I</i> > 2 σ(<i>I</i>)]	3684	3441
No of parameters	262	262
R(int)	0.024	0.048
R1, wR2 (all data)	0.0309, 0.0802	0.0522, 0.1201
R1, wR2 ([<i>I</i> > 2 σ(<i>I</i>)])	0.0299, 0.0796	0.0443, 0.1138
Residual Electron Density (eÅ ⁻³)	0.443, -0.301	0.709, -0.553

Table 2: Selected bond lengths (Å) of complexes **1** and **2**.

	Complex 1	Complex 2
Co(1)–O(1)	1.873(3)	1.886(2)
Co(1)–O(2)	1.914(2)	1.879(2)
Co(1)–O(3)	1.919(2)	1.909(2)
Co(1)–N(1)	1.880(3)	1.870(2)
Co(1)–N(2)	2.025(4)	2.042(2)
Co(1)–N(3)	1.949(3)	1.890(3)

Table 3: Selected bond angles ($^{\circ}$) of complexes **1** and **2**.

	Complex 1	Complex 2
O(1)–Co(1)–O(2)	88.44(12)	88.51(9)
O(1)–Co(1)–O(3)	86.92(12)	89.82(8)
O(1)–Co(1)–N(1)	94.22(13)	91.73(9)
O(1)–Co(1)–N(2)	179.09(16)	178.27(9)
O(1)–Co(1)–N(3)	90.15(12)	89.68(10)
O(2)–Co(1)–O(3)	94.79(10)	94.48(9)
O(2)–Co(1)–N(1)	177.20(12)	86.63(9)
O(2)–Co(1)–N(2)	90.65(15)	91.73(10)
O(2)–Co(1)–N(3)	87.79(13)	175.39(10)
O(3)–Co(1)–N(1)	86.25(11)	178.11(10)
O(3)–Co(1)–N(2)	93.18(13)	91.87(9)
O(3)–Co(1)–N(3)	176.04(13)	89.75(10)
N(1)–Co(1)–N(2)	86.70(16)	86.58(10)
N(1)–Co(1)–N(3)	91.31(14)	89.18(10)
N(2)–Co(1)–N(3)	89.78(14)	89.95(11)

Table 4: Geometric features (distances in Å and angles in °) of N $\cdots\pi$ and C-H $\cdots\pi$ interactions present in solid state the complexes.

Complexes	C-H \cdots Cg(Ring)	X \cdots Cg (Å)	Y-X \cdots Cg (°)	Y \cdots Cg (Å)
1	N(5) \cdots Cg(2)	3.166(4)	54.5(2)	2.668(3)
2	C(14)-H(14B) \cdots Cg(3)	2.60	101	2.936(4)
	C(11)-H(11) \cdots Cg(3) ^a	2.97	142	3.745(3)

Symmetry transformations: ^a = X,1/2-Y,-1/2+Z.

For complex 1:

Cg2 = Centre of gravity of the ring [Co(1)-N(1)-C(11)-C(5)-C(6)-O(1)].

For complex 2:

Cg3 = Centre of gravity of the ring [Co(1)-O(2)-C(17)-C(18)-C(19)-O(3)].

Table 5: Kinetic parameters of both complexes for catechol oxidase mimicking activity using various enzyme kinetic plots at 25° C in acetonitrile medium.

Enzyme kinetic plots	$V_{\max} \pm \text{SE} \text{ (M S}^{-1}\text{)}$		$K_M \pm \text{SE} \text{ (M)}$		$k_{\text{cat}} \pm \text{SE} \text{ (S}^{-1}\text{)}$		$k_{\text{cat}}/K_M \pm \text{SE} \text{ (S}^{-1} \text{M}^{-1}\text{)}$	
	1	2	1	2	1	2	1	2
Lineweaver-Burk plot	$(0.514 \pm 0.122) \times 10^{-5}$	$(0.564 \pm 0.044) \times 10^{-5}$	$(243.203 \pm 14.501) \times 10^{-4}$	$(267.036 \pm 2.691) \times 10^{-4}$	$(0.514 \pm 0.122) \times 10^{-1}$	$(0.564 \pm 0.044) \times 10^{-1}$	$(0.021 \pm 0.002) \times 10^{+2}$	$(0.021 \pm 0.002) \times 10^{+2}$
Hanes-Woolf plot	$(0.514 \pm 0.047) \times 10^{-5}$	$(0.563 \pm 0.061) \times 10^{-5}$	$(243.203 \pm 2.652) \times 10^{-4}$	$(266.563 \pm 3.730) \times 10^{-4}$	$(0.514 \pm 0.047) \times 10^{-1}$	$(0.563 \pm 0.061) \times 10^{-1}$	$(0.021 \pm 0.002) \times 10^{+2}$	$(0.021 \pm 0.002) \times 10^{+2}$
Eadie-Hofstee plot	$(0.484 \pm 0.020) \times 10^{-5}$	$(0.569 \pm 0.029) \times 10^{-5}$	$(226.100 \pm 10.500) \times 10^{-4}$	$(270.200 \pm 15.600) \times 10^{-4}$	$(0.484 \pm 0.020) \times 10^{-1}$	$(0.569 \pm 0.029) \times 10^{-1}$	$(0.021 \pm 0.002) \times 10^{+2}$	$(0.021 \pm 0.002) \times 10^{+2}$

Table 6: Kinetic parameters of both complexes for phenoxazinone synthase mimicking activity using various enzyme kinetic plots at 25° C in acetonitrile medium.

Enzyme kinetic plots	$V_{\max} \pm SE$ (M S ⁻¹)		$K_M \pm SE$ (M)		$k_{cat} \pm SE$ (S ⁻¹)		$k_{cat}/K_M \pm SE$ (S ⁻¹ M ⁻¹)	
	1	2	1	2	1	2	1	2
Lineweaver-Burk plot	(1.181 ± 0.270) x 10 ⁻⁵	(1.295 ± 0.127) x 10 ⁻⁵	(124.136 ± 1.253) x 10 ⁻⁴	(181.814 ± 2.879) x 10 ⁻⁴	(1.181 ± 0.270) x 10 ⁻¹	(1.295 ± 0.127) x 10 ⁻¹	(0.095 ± 0.004) x 10 ⁺²	(0.071 ± 0.002) x 10 ⁺²
Hanes-Woolf plot	(1.181 ± 0.101) x 10 ⁻⁵	(1.294 ± 0.132) x 10 ⁻⁵	(124.147 ± 2.343) x 10 ⁻⁴	(181.729 ± 2.992) x 10 ⁻⁴	(1.181 ± 0.101) x 10 ⁻¹	(1.294 ± 0.132) x 10 ⁻¹	(0.095 ± 0.004) x 10 ⁺²	(0.071 ± 0.002) x 10 ⁺²
Eadie-Hofstee plot	(1.149 ± 0.038) x 10 ⁻⁵	(1.329 ± 0.052) x 10 ⁻⁵	(119.500 ± 0.051) x 10 ⁻⁴	(188.100 ± 0.081) x 10 ⁻⁴	(1.149 ± 0.038) x 10 ⁻¹	(1.329 ± 0.052) x 10 ⁻¹	(0.096 ± 0.007) x 10 ⁺²	(0.071 ± 0.002) x 10 ⁺²

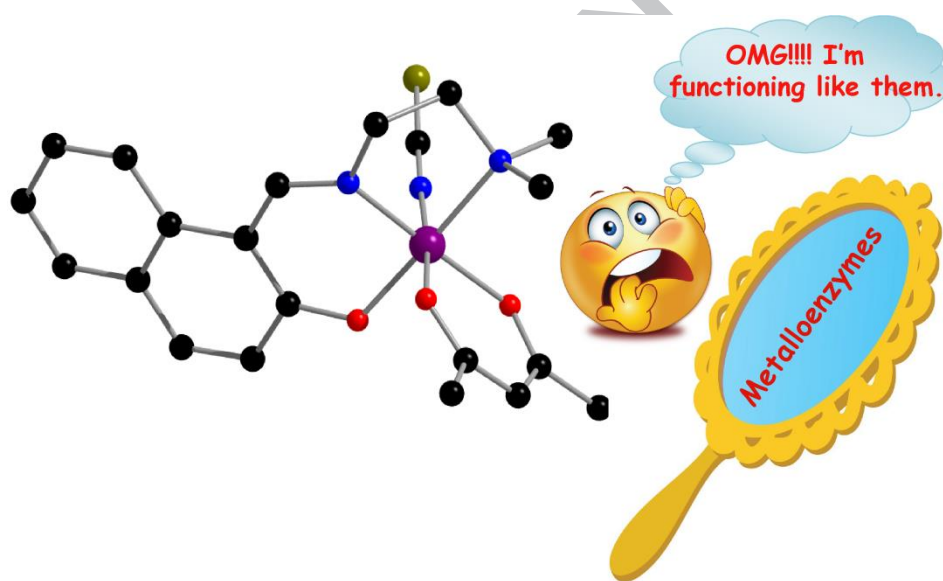
Table 7: Kinetic parameters of both complexes for phosphatase mimicking activity using various enzyme kinetic plots at 25° C in aqueous DMF (98% DMF, v/v) medium.

Enzyme kinetic plots	$V_{\max} \pm \text{SE} \text{ (M S}^{-1}\text{)}$		$K_M \pm \text{SE} \text{ (M)}$		$k_{\text{cat}} \pm \text{SE} \text{ (S}^{-1}\text{)}$		$k_{\text{cat}}/K_M \pm \text{SE} \text{ (S}^{-1} \text{M}^{-1}\text{)}$	
	1	2	1	2	1	2	1	2
Lineweaver-Burk plot	$(0.409 \pm 0.006) \times 10^{-5}$	$(0.446 \pm 0.005) \times 10^{-5}$	$(8.995 \pm 0.003) \times 10^{-4}$	$(11.138 \pm 0.016) \times 10^{-4}$	$(0.409 \pm 0.006) \times 10^{-1}$	$(0.446 \pm 0.005) \times 10^{-1}$	$(0.045 \pm 0.002) \times 10^{+2}$	$(0.04 \pm 0.003) \times 10^{+2}$
Hanes-Woolf plot	$(0.409 \pm 0.006) \times 10^{-5}$	$(0.446 \pm 0.005) \times 10^{-5}$	$(8.995 \pm 0.003) \times 10^{-4}$	$(11.138 \pm 0.016) \times 10^{-4}$	$(0.409 \pm 0.006) \times 10^{-1}$	$(0.446 \pm 0.005) \times 10^{-1}$	$(0.045 \pm 0.002) \times 10^{+2}$	$(0.04 \pm 0.003) \times 10^{+2}$
Eadie-Hofstee plot	$(0.410 \pm 0.006) \times 10^{-5}$	$(0.447 \pm 0.004) \times 10^{-5}$	$(9.046 \pm 0.339) \times 10^{-4}$	$(11.200 \pm 0.236) \times 10^{-4}$	$(0.410 \pm 0.006) \times 10^{-1}$	$(0.447 \pm 0.004) \times 10^{-1}$	$(0.045 \pm 0.002) \times 10^{+2}$	$(0.04 \pm 0.002) \times 10^{+2}$

Graphical Abstract (Pictogram)

Synthetic stratagem and structures of two heteroleptic cobalt(III) complexes acting as biomimetic catalysts: Role of co-ligands in catalytic activities

Kousik Ghosh, Shouvik Chattopadhyay



Graphical Abstract (Synopsis)

Synthetic stratagem and structures of two heteroleptic cobalt(III) complexes acting as biomimetic catalysts: Role of co-ligands in catalytic activities

Kousik Ghosh, Shouvik Chattopadhyay

Two mixed ligand cobalt(III) complexes have been synthesized and characterized and used to mimic the role of catechol oxidase, phenoxazinone synthase and phosphatase efficiently. The catalytic activity of complex **2** (towards all these bio-relevant catalyses) is higher compared to complex **1**. This may be correlated with the presence of easily replaceable thiocyanate in **2** (compared to azide in **1**) initiating the catalytic cycle by forming stable catalyst-substrate adduct easily.